Journal of Chromatography A, 1216 (2009) 967–976

Contents lists available at ScienceDirect

Journal of Chromatography A

journal homepage: www.elsevier.com/locate/chroma

Serial displacement chromatofocusing and its applications in multidimensional chromatography and gel electrophoresis: I. Theory and general considerations

Hong Shen [1], Douglas D. Frey *

Department of Chemical and Biochemical Engineering, University of Maryland Baltimore County, Baltimore, MD 21250, USA

ARTICLE INFO

Article history:
Received 18 October 2008
Received in revised form
26 November 2008
Accepted 27 November 2008
Available online 6 December 2008

Keywords:
Chromatofocusing
Serial displacement chromatofocusing
Proteins
Peptides

ABSTRACT

The technique of "serial displacement chromatofocusing" (SDC) is investigated both theoretically and experimentally with model mixtures of proteins and peptides. The method employs a multistep, retained pH gradient formed using adsorbed buffering species to produce a series of discrete effluent fractions. Each of these fractions may contain several displaced protein bands under conditions of sufficient mass overloading, so that several displacement trains of adjoined bands can be produced in a single chromatographic run. Numerical simulations and experimental results showed selective concentration effects for minor components in a fraction when the feed amount was sufficient large. A computer-aided design method was developed to facilitate the use of the method and was applied to both anion- and cation-exchange column packings. Good agreement was achieved between the designed pH gradients and experimental results. The characteristics of SDC were also explored in terms of its loading capacity, scalability, repeatability, recovery, and differentiation of proteins between their true and apparent isoelectric point values.

1. Introduction

Chromatofocusing is a version of ion-exchange chromatography which employs an internally generated, retained pH gradient. The method combines many of the most favorable characteristics of ion-exchange chromatography and isoelectric focusing (IEF) [1,2], so that it is reasonable to investigate its use as an alternative to these two methods in a variety of analytical applications, including in the proteomics area. Traditional chromatofocusing techniques employing a polyampholyte buffer have two major shortcomings which greatly limited its use in practice. One shortcoming is the use of polyampholyte elution buffers, which often exhibit lot-to-lot variations in composition which may affect the repeatability of the method [3]. Polyampholytes also tend to form association complexes with proteins [4,5], which may complicate subsequent procedures, such as reversed-phase chromatography, mass spectrometry [6] or gel staining [7]. A second shortcoming is that a column packing with a uniform buffering capacity over a broad pH range has traditionally been used, in which case the choices for the packing are limited. However, it has been shown that under appropriate conditions, chromatofocusing can be performed on nearly any type of ion-exchange column packing so that a larger variety of commercially available packings that have advantageous characteristics for a given application can be better exploited [8–10].

In Part I of this study, a variant of the chromatofocusing technique, termed "serial displacement chromatofocusing" (SDC), will be investigated theoretically and experimentally using model proteins and peptides. SDC involves the elution or displacement of proteins or peptides using a multistep, retained pH gradient formed using simple mixtures of buffering species instead of polyampholytes. Previous work has demonstrated that a single self-sharpening, retained pH front can function as a protein displacer to accomplish displacement chromatography [11]. In the present work, this method will be extended to the case of multiple pH fronts in a single chromatographic run. In Part II of this study, the usefulness of the SDC method will be assessed in specific systems employing two-dimensional polyacrylamide gel electrophoresis (2D-PAGE) and two-dimensional high-performance liquid chromatography (2D-HPLC).

2. Experimental

Human hemoglobin variants A, F, S, and C were obtained from Perkin-Elmer (Wallasley, MA, USA). IgG was a gift from W.R. Grace (Columbia, MD, USA). Trypsin Gold was obtained from Promega (Madison, WI, USA). All other proteins were obtained from Sigma (St. Louis, MO, USA). A protease inhibitor cocktail was obtained from Roche (Indianapolis, IN, USA). All chemicals were obtained from Sigma–Aldrich, except for formic acid, which was obtained from J.T.

* Corresponding author. Tel.: +1 410 455 3418; fax: +1 410 455 6500.
E-mail address: dfrey1@umbc.edu (D.D. Frey).
[1] Present address: Centocor, 200 Great Valley Parkway, Malvern, PA 19355, USA.

0021-9673/$ – see front matter © 2008 Elsevier B.V. All rights reserved.
doi:10.1016/j.chroma.2008.11.086

Baker (Philipsburg, NJ, USA). All buffer compositions are described in the figure captions, and the buffer solutions were prepared using deionized water which was vacuum filtered using a 47-mm diameter nylon membrane filter with 0.2-μm pores (Whatman, Clifton, NJ, USA).

A 7.5 cm × 0.75 cm I.D. TSK-GEL Q-5PW strong-base ion-exchange column and a 7.5 cm × 0.75 cm I.D. TSK-GEL SP-5PW strong-acid ion-exchange column were obtained from Tosoh Bioscience (Montgomeryville, PA, USA). A 25 cm × 0.4 cm I.D. and a 25 cm × 0.1 cm I.D. ProPac SAX-10 strong-base ion-exchange column were gifts from Dionex (Sunnyvale, CA, USA). A 5 cm × 0.5 cm I.D. Mono P HR 5/5 weak-base ion-exchange column was obtained from GE Healthcare (Piscataway, NJ, USA).

Experiments were performed using an Ultimate HPLC instrument from Dionex, and both conventional and micro UZ-view flow cells having volumes of 10 μL and 180 nL, respectively, were employed for UV detections at different scales. The column effluent was monitored at both 280 and 415 nm. The UZ-view flow cell was connected to a poly(vinylidene difluoride) (PVDF) 50 μL internal volume flow cell matched with a 450CD pH electrode (Sensorex, Garden Grove, CA, USA) so that the pH of the column effluent could be directly measured. Digital pH signals were formed within a series network composed of a pH electrode, an Orion 520A pH meter (Orion, Beverly, MA, USA), and a WellChrom interface box V7566 Version 0696. These signals were then relayed through the interface box into the Ultimate instrument, so that pH and UV absorbance data can be collected simultaneously by the computer every 2 s. The pH meter and electrode were calibrated each time before the experiments at a given pH, and the same pH probe was used for measuring both the elution buffer pH and column effluent pH. All the chromatography experiments were controlled by Chromeleon software version 6.6 from Dionex.

3. Theory

3.1. Adsorption equilibrium

To simplify the following development, consider specifically the case of an anion-exchange column packing. The concentrations of the negatively charged forms of each acidic buffering species in the fluid and adsorbed phases, $C_{A_i^-}$ and $q_{A_i^-}$, are related to the total amounts of a buffering species in those phases, C_{A_i} and q_{A_i}, according to the following acid-base equilibrium relations:

$$C_{A_i^-} = \frac{K_{A_i} C_{A_i}}{C_{H^+} + K_{A_i}} \tag{1}$$

$$q_{A_i^-} = \frac{K_{A_i} q_{A_i}}{q_{H^+} + K_{A_i}} \tag{2}$$

In Eqs. (1) and (2), K_{A_i} is the fluid-phase acid-base dissociation constant, and q_{H^+} and C_{H^+} are the hydrogen ion concentrations in the adsorbed and fluid phases. Adsorption equilibrium for each charged form of each buffering species can be represented by equating the chemical potential of electrically neutral combinations of ions in each phase to arrive at the following relation:

$$(q_{H^+})^{-1} q_{A_i^-} = K_{A_i^-,\mathrm{ads}} (C_{H^+})^{-1} C_{A_i^-} \tag{3}$$

where $K_{A_i^-,\mathrm{ads}}$ is adsorption equilibrium constant. For an uncharged species, the exponents on the hydrogen ion concentrations in Eq. (3) are zero so that a linear equilibrium relation results. The protein charge can be represented empirically as a linear function of the fluid phase pH according to

$$z_P = a(\mathrm{pH}_{\mathrm{ref}} - \mathrm{pH}_{\mathrm{fluid}}) \tag{4}$$

where $\mathrm{pH}_{\mathrm{fluid,ref}}$ is the fluid phase pH when $z_P = 0$, and z_P is the characteristic binding charge that determines the protein adsorption equilibrium. Protein adsorption equilibrium can then be represented in a manner analogous to Eq. (3) as

$$(q_{H^+})^{-z_P} q_P = K_{P,\mathrm{ads}} (C_{H^+})^{-z_P} C_P \tag{5}$$

The electroneutrality condition in the liquid and adsorbed phases can be expressed using Eqs. (1) and (2) to yield

$$C_{Na^+} - \sum_{i=1}^{n} \frac{K_{A_i} C_{A_i}}{K_{A_i} + C_{H^+}} + \sum_{i=1}^{m} \frac{C_{H^+} C_{B_i}}{K_{B_i} + C_{H^+}} + \sum_{i=1}^{e} z_{P_i} C_{P_i} + C_{H^+} - \frac{K_W}{C_{H^+}} = 0 \tag{6}$$

$$q_{Na^+} - \sum_{i=1}^{n} \frac{K_{A_i} q_{A_i}}{K_{A_i} + C_{H^+}} + \sum_{i=1}^{l} \frac{q_{H^+} q_{R_i}}{K_{R_i} + q_{H^+}} + \sum_{i=1}^{e} z_{P_i} q_{P_i} + q_{H^+} - \frac{K_W}{q_{H^+}} = 0 \tag{7}$$

In Eqs. (6) and (7), A_i and B_i represent acidic and basic buffering species, q_{R_i} is the concentration of the ion-exchange functional group R_i, and K_W is the ionic product of water.

As described by Frey et al. [12], for a specified liquid-phase, Eqs. (1)–(7) can be solved for the equilibrium adsorbed-phase composition. However, in general the maximum ion-exchange adsorption capacity observed experimentally for a protein is much less than q_{R^+}/z_P, where q_{R^+} is the total concentration of ion-exchange functional groups on the column packing, since a large fraction of these functional groups are located directly underneath an adsorbed protein and are therefore sterically blocked from participating in ion-exchange equilibrium. This was accounted for in this study using a steric factor, defined as the number of sterically blocked functional groups on the column packing due to the adsorption of one protein [13,14]. This steric factor was incorporated into the calculation using the method developed by Strong [15], as described in Appendix A.

3.2. Computer-aided design method for "engineering" a multistep, retained pH gradient

In this section, a modified version of the local-equilibrium theory developed by Frey et al. [9] is employed to determine the shape of the pH gradient for a specified eluent composition and for specified physical properties of the buffering species. As in the preceding section, to simplify the following development, the relations are presented specifically for an anion-exchange column packing although with appropriate modifications they can also be applied to a cation-exchange column packing. Note that certain of the relations presented here have been adapted from Frey et al., from which additional details concerning the method can be obtained.

It is assumed that the column is initially equilibrated with a presaturation buffer at a high pH value produced by titrating a certain amount of NaOH dissolved in water with the weak-acid buffering species having the highest pK_{A_i} value from among the buffering species present in both the presaturation and elution buffers. Subsequently, an elution buffer at a low pH value is introduced into the column as a step change at the column entrance. This buffer is assumed to have the same Na^+ concentration as in the presaturation buffer, but it is titrated with a mixture of weak-acid buffering species to the desired pH. Due to the acid-base and adsorption equilibrium behavior of this system, a multistep, retained pH gradient becomes self-generated inside the column.

According to local-equilibrium theory, the velocity of a self-sharpening front which spans the compositions between an upstream and downstream composition plateau is given by [16]

$$v_{\Delta C} = \frac{v_{\mathrm{fluid}}}{1 + \frac{(1-\alpha)\varepsilon}{\alpha} + \frac{(1-\alpha)(1-\varepsilon)}{\alpha} \left[\frac{q_{A_i,u} - q_{A_i,d}}{C_{A_i,u} - C_{A_i,d}} \right]} \tag{8}$$

where $v_{\Delta C}$ is the velocity of a concentration change, v_{fluid} is the interstitial velocity of fluid phase, the subscripts u and d denote the upstream and downstream composition plateaus, respectively, and the various other variables are defined in the symbols section. Coherence theory [9,17] can be applied by assuming that a stepwise composition change continues to span a fixed composition range for every component as it travels downstream. For any two buffering species on a particular pH front it follows from Eq. (8) and the coherence condition just stated that

$$\frac{q_{A_i,u} - q_{A_i,d}}{C_{A_i,u} - C_{A_i,d}} = \frac{q_{A_j,u} - q_{A_j,d}}{C_{A_j,u} - C_{A_j,d}} \quad (9)$$

The relations just described are convenient to solve only if certain features of the pH gradient are known *ab initio*, such as the number of pH fronts that are formed and the buffering species that appear or disappear on each front. Rules for obtaining this information are given in Appendix B. Consider the case where there are n_a acidic buffering species present in the elution profile. According to Appendix B, in this case there will be $n_a(n_a - 1)/2$ unknown values of C_{A_i} on the $n_a - 1$ intermediate plateaus that are formed. These values can be solved for using an equal number of independent coherence conditions of the type given by Eq. (9), where q_{A_i} is related to C_{A_i} according to the relations in Section 3.1. Since the pH values of the presaturation and elution buffers are assumed to be known, the electroneutrality conditions in the fluid phase for both presaturation and elution plateaus can be used to calculate the concentrations of the titrating buffering species in both buffers. The remaining $2(n_a - 1)$ unknown values of pH in both phases can then be solved for by using an equal number of independent electroneutrality conditions as shown in Eqs. (6) and (7).

To determine the values of the physical properties needed, such as the adsorption equilibrium constants for the buffering species, one or more "training" experiments were conducted to produce several pH gradient shapes, each of which were represented using $2(n_f + 1)$ data points that best describe the shape of the gradient, where n_f is the number of retained pH fronts. The physical properties were considered as adjustable parameters that were the same for the training experiments and the design calculations, and the local-equilibrium theory equations were then solved simultaneously while also minimizing the following objective function:

$$F = \sum_{i=1}^{n_{\text{case}}} \sum_{j=1}^{2(n_f+1)} (t_{\text{fit}} - t_{\text{exp}})_{i,j}^2 + (\text{pH}_{\text{fit}} - \text{pH}_{\text{exp}})_{i,j}^2 \quad (10)$$

where t and pH are the elution time and pH at the representative point, respectively, and subscripts "fit" and "exp" denote the fitted and experimental values, respectively. After the set of physical properties was determined, a desired pH gradient was designed by solving an optimization problem in which the concentrations of the buffering species in the elution and presaturation buffers are used as adjustable variables, and the objective function is defined similarly to Eq. (10), but as the difference between the predicted and desired pH gradient.

The use of the computer-aided design method for producing multistep, retained pH gradients is illustrated in Fig. 1 where two "training" experiments were performed. To facilitate the determination of the physical properties, some of the properties, such as $K_{\text{Na,ads}}$, which are not critical for the optimization problem, were given reasonable fixed values as listed in the figure caption. Other physical properties, such as column length (L) and column diameter (D), were known, and the remaining physical properties were used as adjustable parameters. In addition, the allowable range for the buffering species adsorption equilibrium constants, $K_{A_i,\text{ads}}$, was assumed to be between 0.2 and 5 to further facilitate the search algorithm. During the fitting procedure, it was observed that the adsorption equilibrium constants for the positively charged forms

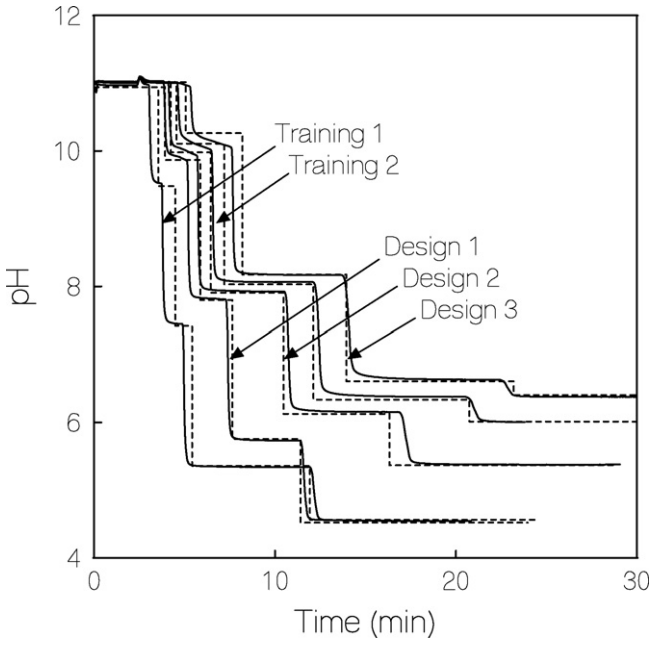

Fig. 1. Theoretical (dotted curve) and experimental (solid curve) pH gradients formed on the ProPac SAX-10 column (25 cm × 0.4 cm I.D.). The presaturation buffer was the same for each case and contained 20 mM NaOH titrated with CAPS to pH 11. The elution buffer for training experiment 1 contained 20 mM NaOH, 40 mM TAPS, and 20 mM MES titrated with acetic acid to pH 4.6. The elution buffer for training experiment 2 contained 20 mM NaOH, 100 mM TAPS, and 100 mM MES titrated with acetic acid to pH 6.0. The elution buffer for designed gradient 1 contained 20 mM NaOH, 44 mM TAPS, and 30 mM MES titrated with acetic acid to pH 4.5. The elution buffer for designed gradient 2 contained 20 mM NaOH, 50 mM TAPS, and 19 mM MES titrated with acetic acid to pH 5.4. The elution buffer for designed gradient 3 contained 20 mM NaOH, 31 mM TAPS, and 18 mM MES titrated with acetic acid to pH 6.4. The flow rate was 0.5 mL/min. The physical properties used were $L = 25$ cm, $D = 0.4$ cm, $q_R = 0.079$ mol/L, $\alpha = 0.4$, $\varepsilon = 0$, $K_{\text{CAPS}^0,\text{ads}} = K_{\text{TAPS}^0,\text{ads}} = K_{\text{MES}^0,\text{ads}} = 0.20$, $K_{\text{HAc}^0,\text{ads}} = 1.42$, $K_{\text{CAPS}^-,\text{ads}} = 0.20$, $K_{\text{TAPS}^-,\text{ads}} = 0.92$, $K_{\text{MES}^-,\text{ads}} = 0.90$, $K_{\text{HAc}^-,\text{ads}} = 1.75$, $K_{\text{Na}^+,\text{ads}} = 1.0$.

of the buffering species did not affect the calculation significantly since the adsorbed phase concentrations of these species are negligible for the column packing employed. These constants were therefore given values of unity. After the physical properties were determined, they were used to design several pH gradients. As shown in Fig. 1, the experimental pH gradients agree well with the desired target gradients, even for target gradients located outside of the range of the training experiments.

Similarly successful results were achieved for several other columns. In particular, Fig. 2 shows an example of the computer-aided design method used to produce a multistep, retained pH gradient on a TSK-GEL SP-5PW column, which is a strong-acid cation-exchange column. In contrast to the previous example, the elution buffer for this case contained a mixture of weak-acid and weak-base buffering species, in which case the weak-base buffering species generated the pH fronts and the weak-acid buffering species, i.e., CHES, served to modify the ionic strength on the pH front. Under these conditions, during the elution process increasing amounts of the weak-acid (i.e., unadsorbed) buffering species are ionized in the upstream direction, which can be exploited, if desired, to increase the focusing effect of the latter pH fronts, or to adjust the protein solubility through ionic strength effects. To achieve the results shown in Fig. 2, the values of α, ε, q_R, $K_{\text{Cl,ads}}$, and $K_{\text{CHES,ads}}$ were set to reasonable values as listed in the figure caption. As illustrated in the figure, good agreement was achieved between the experiments and the theoretical design for the pH gradient, which indicates that the computer-aided design method can be applied to both cation-exchange as well as anion-exchange

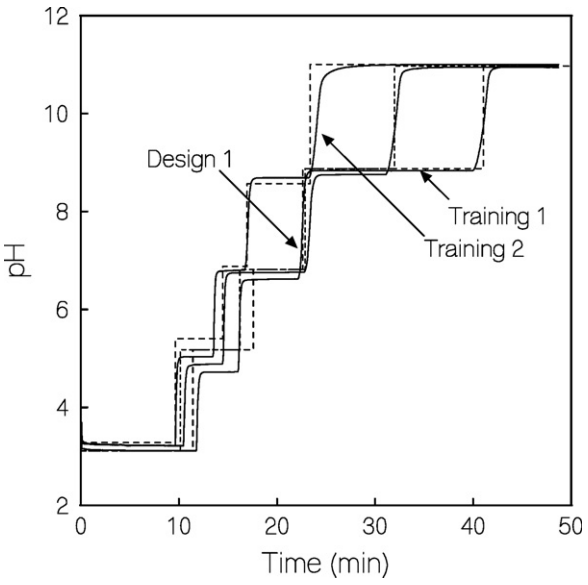

Fig. 2. Comparison of theoretical (dotted curve) and experimental (solid curve) stepwise pH gradients formed on a strong-acid ion-exchange column packing (TSK-GEL SP-5PW). The presaturation buffer was the same for each case and contained 20 mM N,O-dimethylhydroxylamine-HCl, pH 3.2. The elution buffer for training experiment 1 contained 20 mM HCl, 20 mM BIS-TRIS, 20 mM diethanolamine titrated with NaOH to pH 11. The elution buffer for training experiment 2 contained 20 mM HCl, 20 mM BIS-TRIS, 20 mM diethanolamine, 20 mM TES titrated with NaOH to pH 11. The elution buffer for design gradient 1 contained 20 mM HCl, 7 mM CHES, 29 mM BIS-TRIS, 11 mM diethanolamine titrated with NaOH to pH 11. The flow rate was 0.5 mL/min. The set of physical properties used were $L = 7.5$ cm, $D = 0.75$ cm, $q_R = 0.44$ mol/L, $\alpha = 0.4$, $\varepsilon = 0.6$, $K_{Na^+,ads} = 1.7$, $K_{Bis\text{-}Tris^+,ads} = 4.8$, $K_{diethanolamine^+,ads} = 0.2$, $K_{dimethylhydroxylamine^+,ads} = 0.2$, $K_{Bis\text{-}Tris^0,ads} = 0.2$, $K_{diethanolamine^0,ads} = 0.2$, $K_{dimethylhydroxylamine^0,ads} = 2.0$, $K_{Cl^-,ads} = 1.0$, $K_{CHES^0,ads} = K_{CHES^{-1},ads} = 1.0$.

column packings. Finally, it should be noted that twelve general purpose buffer and column packing "recipes" described by Shen et al. [18], some of which were also used by Brorson et al. [19], can be employed as starting points for a pH gradient. The computer-aided design method described here can then be used to further optimize the gradient shape for a specific application.

3.3. Studies of the separation and selective concentration behavior of minor components in SDC

When large numbers of different components are present at a certain pH front in SDC, usually relatively few, and possibly just one, of the components are present in sufficient amounts to form fully rectangular displaced bands. Furthermore, it is often the case that the low-abundance components not forming rectangular displaced bands will be of primary interest in proteomics applications since they tend to be the components directly involved in cellular behavior, an example being the regulatory proteins. Although the ability of displacement chromatography to selectively concentrate a minor component and thereby enhance their detection has been discussed previously [20,21], this past work has not addressed the particular case where SDC is employed and where some or all of the components may be present in amounts that are insufficient to form fully rectangular displaced bands. Consequently, in this section both experiments and numerical simulations using the numerical method of characteristics as described by Frey et al. [12] were conducted in order to illustrate the behavior of minor components in SDC. To perform the simulations, mass-transfer rates were approximated using a linear driving force approximation as follows:

$$dq_i/dt = (60D_i/d_P^2)(q_i - q_i^*) \quad (11)$$

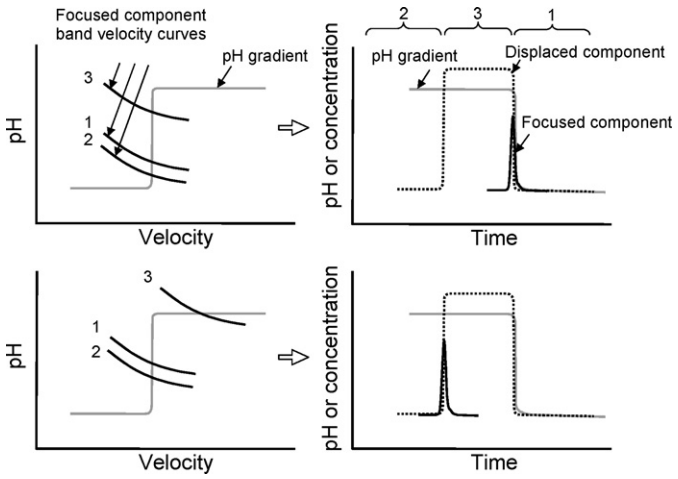

Fig. 3. Location of a minor band (dark solid curve) in the presence of a major band (dark dotted curve) co-eluted on a retained pH front. The left panels show the band velocity curves of a trace peak of the minor component for the three particular regions denoted on the right panels.

where q_i^* is the adsorbed-phase concentration of component i that would be in equilibrium with the prevailing fluid-phase composition, and D_i is the diffusion coefficient of component i. The adsorption equilibrium relations used in the numerical simulations were those described in Section 3.1.

Fig. 3 illustrates qualitative criteria that determine the location of a minor component in the presence of a major component that forms a rectangular band during SDC. In particular, the left panels show the band velocity curves for the minor component, i.e., the functional relation between the pH and the velocity of a trace band, for three particular regions: (1) the upstream pH plateau, (2) the downstream pH plateau in the absence of the major component being displaced, and (3) the downstream pH plateau in the presence of the major component being displaced. Note that the band velocity curves shown reflect the fact that the presence of the major component in region 3 suppresses the adsorption equilibrium constant of the minor component in that same region, so that the band velocity curve is correspondingly raised, and that a lower salt concentration applies in region 2 as compared to region 1, as discussed below, which lowers the band velocity curve in the former region as compared to the latter region.

Considering the top two panels in Fig. 3 where the three band velocity curves intersect the vertical section of pH profile, it can be seen that a trace amount of minor component present on the upstream plateau would have a velocity greater than the pH front, while a trace amount of protein present in region 3 would have a velocity less than the pH front, so the minor component focuses on the pH front itself. The second panel on the left side of Fig. 3 illustrates an alternative case where the positions of band velocity curves 1 and 2 ensure that the minor component will focus as a band between regions 1 and 2, but where the location of band velocity curve 3 precludes the minor component from focusing at the pH front since in this case the velocity of a trace band of the minor component in region 3 would have a velocity greater than the pH front. Consequently, the minor component will focus as a narrow band at the border between regions 2 and 3.

Fig. 4 illustrates numerical calculations of the behavior of a minor component in the presence of a major component in SDC corresponding to the bottom two panels in Fig. 3. In the simulations, the ratio of the amounts of the two components in the feed sample is fixed at four, but the total amount of the two components in the feed sample is varied. As shown in panel A, when the feed sample amount is small, both components focus as narrow bands on the

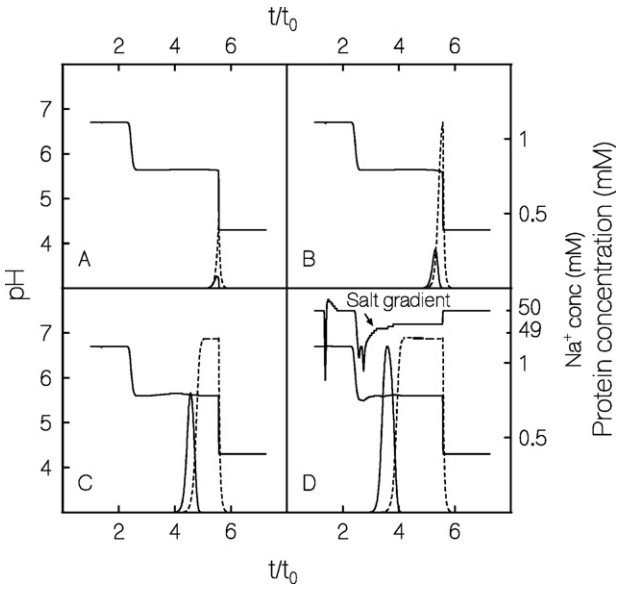

Fig. 4. Calculated behavior of a minor component (solid curve) focused at the downstream side of a major component band (dotted curve) in SDC. The concentration ratio for the major and minor components was 4, and the total sample amounts are in the ratio of 1:4:16:32 for panels A, B, C, and D, respectively. The presaturation buffer contained 50 mM NaOH titrated with MES to pH 6.7, and the elution buffer contained 50 mM NaOH and 208 mM acetic acid at pH 4.3. The interstitial fluid velocity was 0.05 cm/s, and $L = 24$ cm, $d_p = 90$ μm, $q_R = 0.35$ mol/L, $\alpha = 0.35$, and $\varepsilon = 0$. K_{ads} for MES was 0.8 and all the other values of K_{ads} were unity. The diffusivities in the particles for Na^+, Ac^-, MES^-, H^+, and OH^- were 4.6×10^{-6}, 4.1×10^{-6}, 3.4×10^{-6}, 6.5×10^{-6}, 1.0×10^{-6} cm^2/s, respectively, and the diffusivities for both proteins were 1.0×10^{-7} cm^2/s. The values used in Eq. (4) were $a = 4$ and $pH_{ref} = 4$ for the major component and $pH_{ref} = 4.5$ for the minor component.

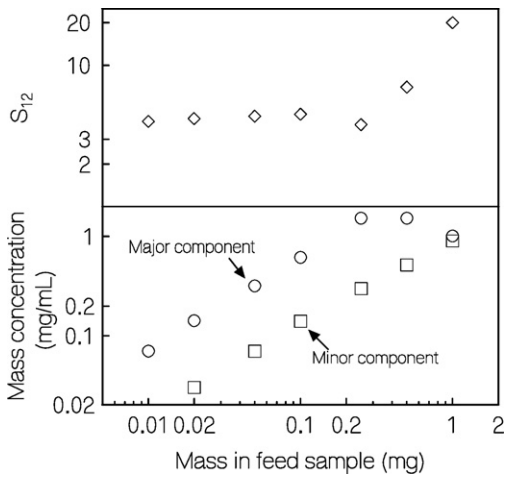

Fig. 5. Experimental results for the selective concentration effect for a feed sample containing 5% (m/v) bovine cytochrome *c* and 95% (m/v) Gly-Gly-Tyr-Arg eluted on a pH front in SDC and simulation results (bottom panel) for the selective concentration effect based on the conditions shown in Fig. 4. Top: selective concentration factor versus mass in feed sample. Middle: mass concentration in the effluent versus mass in feed sample.

pH front, in which case the ratio of the maximum concentrations of the two components in the column effluent is determined by their respective band-broadening (i.e., mass-transfer) properties and the relative positions of the band velocity curves. Fig. 4 shows that as the total amount of sample increases, a significant selective concentration effect is attained well before the minor component forms a fully rectangular band, and some selective concentration of the minor component is attained even when none of the components present form fully rectangular bands. However, as also shown, the maximum selective concentration effect occurs when both minor and major components form fully rectangular bands, in which case both component bands are characterized by near saturation conditions in the adsorbed phase. In this case, since both bands have the same velocity, and therefore the same distribution ratio given as q_{P_i}/C_{P_i}, then the ratio of the fluid-phase molar concentrations of the two components becomes nearly equal to the inverse ratio of their steric factors (see Appendix A), since for both components at saturation $q_{P_i} \cong q_{R^+}/\sigma_i$. Finally, as shown in panel D in Fig. 4, the change in ionic strength near the second pH front, as indicated by the concentration of Na^+, is much smaller than, and in the opposite direction in comparison to, the induced salt gradient produced by a traditional low-molecular-weight displacer in displacement chromatography [22]. This characteristic may be advantageous in SDC since a low ionic strength in the vicinity of the displaced proteins promotes their solubility. Experimental results (data not shown) qualitatively confirmed these trends in ionic strength changes.

A selective concentration factor for component *i*, S_{ij}, can be defined as the ratio of the maximum concentrations of component *i* and a second comparison component *j* in the column effluent divided by this same ratio in the feed sample. When both components are present in small amounts, S_{ij} is near unity and is a function of the component diffusivities, as illustrated in panel A of Fig. 4. Conversely, when the feed amount is sufficiently large that rectangular bands are formed for both components, the ratio of the maximum concentrations of the two components in the effluent becomes approximately equal to the inverse ratio of their respective steric factors as described above, so that $S_{ij,max} \approx (C_{j,f}/C_{i,f}) \times (\sigma_j/\sigma_i)$.

Since protein steric factors are approximately proportional to the protein cross-sectional area, and therefore approximately proportional to the 2/3 power of the relative protein molecular mass, it follows from above that $S_{ij,max} \approx (m_{j,f}/m_{i,f}) \times (M_{r,i}/M_{r,j})^{1/3}$, where *m* denotes the mass concentration. In qualitative support of this relation, Fig. 5 shows experimental results for the selective concentration of a minor component at a retained pH front where the ratio of the relative molecular mass of the minor and major components was 25 and the mass ratio of these components in the feed was 1:20. As shown in the top panel of the figure, the largest value of S_{ij} observed was approximately 20, which is somewhat smaller than the predicted maximum possible value of $20 \times 25^{1/3} = 58$. This is evidently due to the fact that the maximum feed sample size used was not sufficient to form a fully rectangular band for the minor component, as indicated by the trends in the individual component concentrations shown in the bottom panel of Fig. 5. For comparison, Fig. 6 illustrates the calculated selective concentration factors for the minor component in Fig. 4 for two ratios of the species diffusion coefficients, and as a function of the feed sample size normalized by the column static capacity. Note finally that Wilkins et al. [20] employed minor and major peptide components with relative molecular mass of 1634 and 357, respectively, a mass feed ratio of 1:250, and a traditional mode of displacement chromatography to achieve a value for S_{ij} of 305, which is only slightly smaller than the predicted maximum possible value of $250 \times (1634/357)^{1/3} = 414$.

The degree to which the selective concentration effect illustrated in Figs. 4 and 5 can be exploited in practice depends on how the fractions obtained from SDC are subsequently used. For example, this effect is completely lost if an entire fraction associated with a pH front is mixed together, which is the case when SDC is coupled to 2D-PAGE, as described in Part II of this study. Alternatively, in the 2D-HPLC method also considered in Part II of this study, where entire fractions localized at a pH front in SDC are sent to a trap column from which individual components are eluted and then introduced into another column, the selective concentration effect achieved in SDC reduces the volume overloading in the second column, so that more concentrated minor components bands are achieved in the overall process.

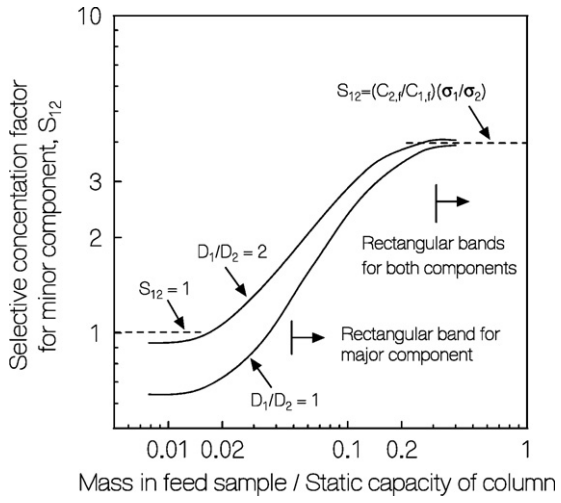

Fig. 6. Relation between the selective concentration factor for the minor component and the total sample mass for the simulations in Fig. 4.

4. Results and discussion

4.1. General characteristics of SDC: loading capacity, scalability, band shape, repeatability, and differentiation of protein in terms of their isoelectric points

As mentioned earlier, one useful feature of chromatofocusing is that proteins elute generally in the order of their true isoelectric points (p*I*) values due to the low and nearly constant ionic strength that exists, and because proteins are only weakly adsorbed during their entire transit time through the column. In order to explore this feature experimentally, proteins with known p*I* values were investigated using an eight-step pH gradient, as shown in Fig. 7

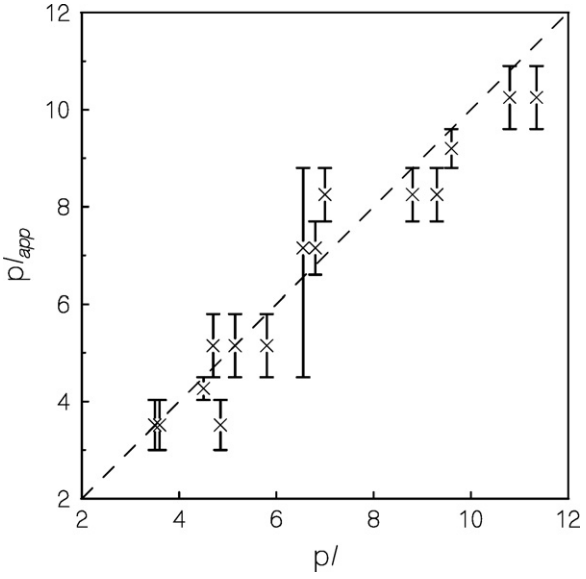

Fig. 7. Relation between protein p*I* and pI_{app} values obtained from an eight-step pH gradient formed on a TSKgel Q-5PW column. The cross symbols represent the middle pH value of the front where the protein eluted, and the solid vertical line represents the pH range that the major protein band spanned on the pH gradient. The dashed line corresponds to $pI = pI_{app}$. The proteins used were chicken lysozyme (p*I* = 11.4), bovine cytochrome *c* (p*I* = 10.8), bovine α-chymotrypsinogen A (p*I* = 9.6), bovine trypsinogen (p*I* = 9.3), bovine ribonuclease A (p*I* = 8.8), amyloglucosidase from *Rhizopus* sp. (p*I* = 8.2), amylase from bacillus licheniformis (p*I* = 7.0), immunoglobulin G (p*I* = 5.8–7.3), human hemoglobin A_0 (p*I* = 6.8), human albumin (p*I* = 5.8), bovine β-lactoglobulin (p*I* = 5.1–5.2), chicken ovalbumin (p*I* = 4.7), soybean trypsin inhibitor (p*I* = 4.5), bovine β-casein (p*I* = 4.6–5.1), amyloglucosidase from *Aspergillus niger* (p*I* = 3.6), fetal calf fetuin (p*I* = 3.2–3.8).

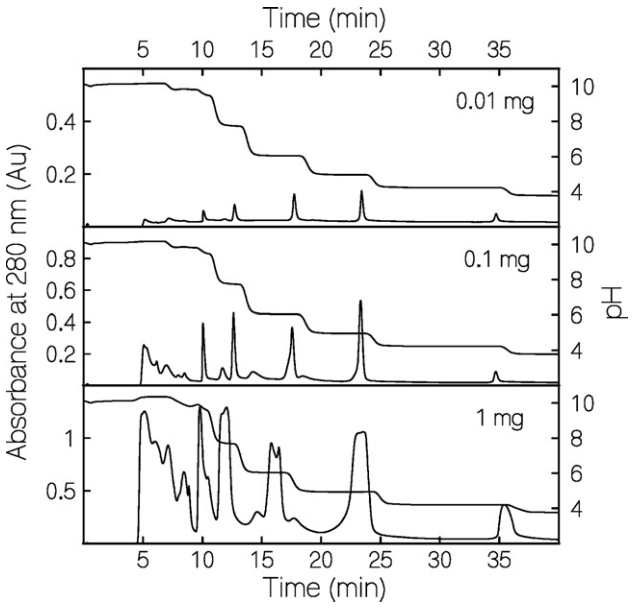

Fig. 8. A protein mixture eluted in a pH gradient formed on a microbore column (ProPac SAX-10, 25 cm × 0.1 cm I.D.). The presaturation buffer contained 20 mM NaOH and 25 mM glycine at pH 10.2, and the elution buffer contained 20 mM NaOH, 30 mM tricine, 20 mM MES, 10 mM acetic acid, and 8.8 mM formic acid titrated with HCl to pH 3.6. The feed sample contained bovine cytochrome *c*, human hemoglobin variants C, S, A, and F, chicken conalbumin, human albumin, bovine β-lactoglobulin A, and amyloglucosidase from *Aspergillus niger*. The flow rate was 30 μL/min, and the absorbance was monitored at 280 nm. All the conditions were the same for the three panels, except for the protein loading amount.

where the *x*-axis refers to either the true reported p*I* of the protein, if the protein is present as a single variant, or the average reported p*I* value of the protein if several variants are present. The *y*-axis refers to the pH range of the front where the protein elutes so that this range also indicates the apparent isoelectric point (pI_{app}) observed in chromatofocusing. As shown, a reasonably linear trend is observed despite the fact that most reported measurements of the true p*I* occur under denaturing conditions [23,24], while native conditions were used for the experiments in Fig. 7. Note that IgG was observed to spread across three fractions in the column effluent, which is evidently due to the polyclonal nature of the IgG used [25]. The results in Fig. 7 can be compared to those of Sluyterman and Wijdenes [2] who employed a polyampholyte elution buffer for chromatofocusing and observed that the true p*I* and the pI_{app} value differed by less than one pH unit for all four proteins that were investigated. Similarly, Zhu et al. [26], who also employed a polyampholyte elution buffer for chromatofocusing, observed that the true p*I* and the pI_{app} value differed by less than one pH unit for 19 of the 23 proteins identified from a breast cancer cell line. The results of Fig. 7 can also compared to a previous study by other workers where an attempt was made to correlate the protein p*I* with the protein elution volume obtained using a linear salt gradient at a fixed pH under non-denaturing conditions where a much less successful correlation was achieved [27].

To investigate the degree to which the sample loading can be varied in SDC, a protein mixture was separated on a six-step pH gradient formed on a micropellicular, strong-base ion-exchange column packing (ProPac SAX-10), and the sample amount was varied from 0.01 to 1 mg for the case of a microbore column with dimensions of 25 cm × 0.1 cm I.D., as shown in Fig. 8, and from 0.1 to 16 mg for the case of a standard analytical column with dimensions of 25 cm × 0.4 cm I.D., as shown in Fig. 9. Note that in Fig. 8 there was a 90-s delay in the elution time for each pH front due to the relatively large dead volume contributed by the pH flow cell as compared to the column volume. The results indicate that the

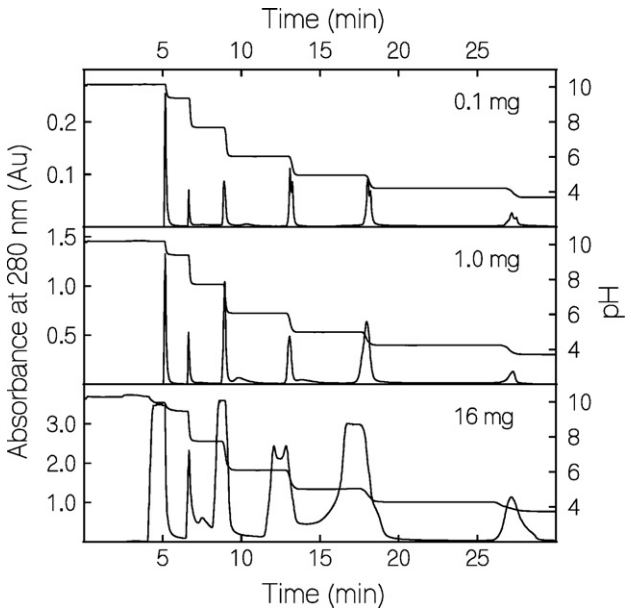

Fig. 9. A protein mixture eluted in a pH gradient formed on a standard diameter column (ProPac SAX-10, 25 cm × 0.4 cm I.D.). The presaturation buffer contained 20 mM NaOH and 25 mM glycine at pH 10.2, and the elution buffer contained 20 mM NaOH, 30 mM tricine, 20 mM MES, 10 mM acetic acid, and 8.8 mM formic acid titrated with HCl to pH 3.6. The feed sample was the same as in Fig. 7. The flow rate was 0.5 mL/min, and the absorbance was monitored at 280 nm. All the conditions used were the same in the three panels, except for the protein loading amount.

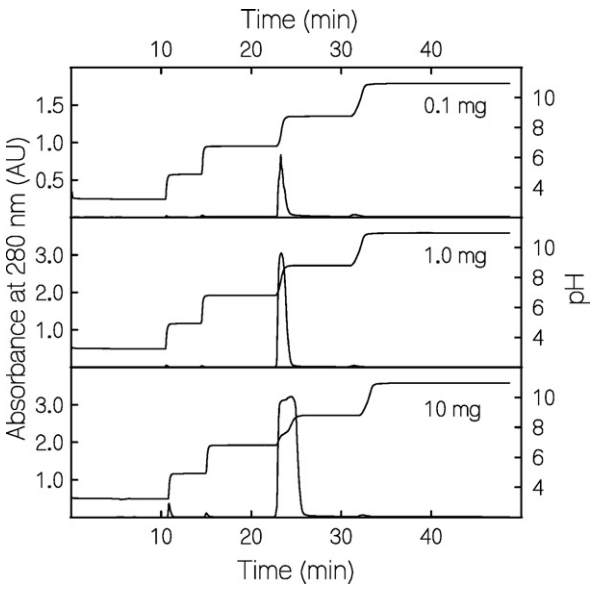

Fig. 10. The peptide Gly-Gly-Tyr-Arg eluted in a pH gradient formed on a TSK-GEL SP-5PW (75 cm × 0.75 cm I.D.) column. The presaturation buffer contained 20 mM N,O-dimethylhydroxylamine hydrochloride at pH 3.2, and the elution buffer contained 20 mM HCl, 7 mM CHES, 29 mM BIS-TRIS, 11 mM diethanolamine titrated with NaOH to pH 11. The flow rate was 0.5 mL/min, and the absorbance was monitored at 280 nm. All the conditions used were the same for the three panels shown above, except for the peptide loading amount.

technique is highly scalable since the peak heights and shapes are similar when the sample mass is inversely related to square of the column diameter. In addition, it can be seen in Figs. 8 and 9 that, under mass-overloaded conditions, displacement development, as indicated by the formation of rectangular protein bands adjoined to a pH front, occurs simultaneously on several different fronts, and in the former case when just 1 mg of protein is used as the feed sample.

Experiments were also performed to demonstrate the applicability of the SDC method to peptides, as shown in Fig. 10, where the pH gradient was designed as described in Fig. 2 and the peptide loading amount was varied from 0.1 to 10 mg. As shown, the peptide could be either focused into a narrow band on a single pH front, or displaced by the pH front to form a rectangular band under the mass-overloaded conditions. The high speed achieved is evident from the fact that the first pH front elutes from the column in only 10 min when the flow rate was 0.5 mL/min. For the case of reversed-phase displacement chromatography using a traditional displacer, it has been reported that the main obstacle in applying this method to peptides is the long separation time, which can be as large as several hours [20]. Fig. 10 indicates that SDC may have applications for achieving displacement separations of peptides on a time scale similar to that achieved by "elution modified" reversed-phase displacement chromatography, which has also been proposed as a means to increase the speed of peptide displacement chromatography [20]. The figure also indicates that when the sample amount was increased to 10 mg, the shape of the pH front where the peptide eluted was affected, evidently due to the high molar concentration of the peptide and the resulting high buffering capacity of the eluent. Nevertheless, the velocities of each pH front and the overall pH gradient shape are still repeatable, and the formation of a displaced, rectangular peptide band is still evident even though the pH varies within the peptide band.

4.2. Peptide and protein recovery in SDC

Four proteins and one peptide, i.e., β-lactoglobulin A, ovalbumin, IgG, cytochrome *c*, and Try-Gly, were eluted individually on a multistep pH gradient, and the effluent fractions were collected and analyzed by size-exclusion chromatography. It has been observed previously that the pH can have a large effect on both the mass recovery and the preservation of biological activity in chromatographic processes [28,29]. Chromatofocusing, however, provides a method for controlling the pH to which a particular protein in the feed sample is exposed so that the recovery of a particular protein can be enhanced. For example, when a stepwise pH front was used to elute cytochrome *c*, the recovery was 88% when the pH front spanned a range of two pH units near the p*I*, but was less than 10% when the front spanned more than 4.5 pH units. In contrast, the recovery of IgG was greater than 95% even when the pH front where the protein eluted spanned 4 pH units. More generally, the average recovery of the four model proteins and the peptide was 90% when the fronts on which the protein was located spans a narrow range near the protein p*I*, which is the normal situation in SDC. Note finally that the recoveries observed here are comparable to, or greater than, those reported for liquid-phase isoelectric focusing or for electrolyzers employing isoelectric membranes [30].

5. Conclusions

A novel serial displacement chromatofocusing (SDC) method in which proteins or peptides are eluted and/or displaced with a multistep, retained pH gradient was investigated along with a computer-aided design method based on local-equilibrium theory. Good agreement was achieved between the designed pH gradients and experimental results. Studies of the method based on both numerical simulations and experiments indicate that SDC can produce a selective concentration effect for minor components in a fraction, that it is repeatable and highly scalable, able to achieve good mass recoveries, and is able to reasonably differentiate proteins in terms of their p*I* values. Specific applications of SDC to 2D-PAGE and 2D-HPLC are considered in Part II of this study.

Symbols

a	constant in Eq. (4)

C component concentration (mol/L)
C_{A_i} concentration of the acidic buffering species A_i in the fluid phase (mol/L)
$C_{A_i^-}$ concentration of the negatively charged form of acidic buffering species A_i^- in the fluid phase (mol/L)
C_{B_i} concentration of the basic buffering species B_i in the fluid phase (mol/L)
$C_{B_i^+}$ concentration of the positively charged form of basic buffering species B_i^+ in the fluid phase (mol/L)
C_{Cl^-} concentration of Cl^- in the fluid phase (mol/L)
C_{H^+} concentration of H^+ in the fluid phase (mol/L)
C_P concentration of protein in the fluid phase (mol/L)
C_{P_i} concentration of protein species P_i in the fluid phase (mol/L)
C_{Na^+} concentration of Na^+ in the adsorbed phase (mol/L)
D column diameter (cm)
D_i diffusion coefficient for component i (cm^2/s)
d_p particle diameter of the column packing (μm)
F objective function
K_{A_i} fluid-phase acid-base dissociation constant of the acidic buffering species A_i (mol/L)
$K_{A_i,ads}$ adsorption equilibrium constant for the acidic buffering species A_i
$K_{A_i^-,ads}$ adsorption equilibrium constant for the negatively charged form of an acidic buffering species A_i^-, such as $CAPS^-$, $TAPS^-$, MES^-, HAc^-, and $CHES^-$
K_{B_i} fluid-phase acid-base dissociation constant of the basic buffering species B_i (mol/L)
$K_{B_i,ads}$ adsorption equilibrium constant for the basic buffering species B_i
$K_{B_i^+,ads}$ adsorption equilibrium constant for the positively charged form of basic buffering species B_{i^+}, such as $Bis\text{-}Tris^+$, $diethanolamine^+$, and $dimethylhydroxylamine^+$
$K_{P,ads}$ adsorption equilibrium constant for the protein
K_{R_i} dissociation constant for the functional group R_i on the column packing (mol/L)
K_W ion product of water ($= 10^{-14} mol^2/L^2$)
L column length (cm)
M_r relative molecular mass
m mass concentration of a substance (g/cm^3)
n moles of adsorption sites per unit mass of adsorbent (mol/g)
n_a number of acidic buffering species present in the elution profile
n_{case} number of cases used in computer-aided design method
n_f number of retained pH fronts
n_{P_i} number of protein species P_i
pH_{fluid} pH in fluid phase
pH_{ref} reference pH where protein charge is zero
pI isoelectric point
pI_{app} apparent isoelectric point
pK_{A_i} the negative logarithm of the fluid-phase acid-base dissociation constant for the acidic buffering species A_i
q_{A_i} concentration of the buffering species A_i in the adsorbed phase (mol/L)
$q_{A_i^-}$ concentration of the negatively charged form of buffering species A_i- in the adsorbed phase (mol/L)
q_{Cl^-} concentration of Cl^- in the adsorbed phase (mol/L)
q_{H^+} concentration of H^+ in the adsorbed phase (mol/L)
q_i concentration of component i in the adsorbed phase (mol/L)
q_{Na^+} concentration of Na^+ in the adsorbed phase (mol/L)
q_P concentration of protein in the adsorbed phase (mol/L)
q_{P_i} concentration of protein species P_i in the adsorbed phase (mol/L)
q_{R_i} concentration of the ionogenic functional group R_i on the column packing (mol/L)
q_{R^+} total concentration of ion-exchange functional groups on the column packing (mol/L)
S_{ij} ratio of the maximum concentration of component i and a second comparison component j in the column effluent divided by this same ratio in the feed sample
t elution time of the pH front (s)
V volume of adsorbed phase per unit mass of adsorbent (L/g)
v_{fluid} interstitial velocity of fluid phase (cm/s)
$v_{\Delta C}$ the velocity of a concentration change (cm/s)
z_P the characteristic binding charge that determines the protein adsorption equilibrium
z_{P_i} the characteristic binding charge that determines the adsorption equilibrium of protein species P_i

Greek symbols
α interparticle void volume of the column
ε intraparticle void volume of the column (particle porosity)
σ steric factor
ψ constant in Eq. (A12)

Subscripts
+, −, 0 charge type
ads adsorbed phase
A_i acidic buffering species
b blocked portion of adsorbed phase, blocked volume used to determine the concentration
B_i basic buffering species
d downstream value
exp experimental values
f feed
fit fitted values
i component i
j component j
max maximum concentrations of the component
P protein
P_i protein species i
R_b blocked adsorption site
R_t total adsorption site
R_u unblocked adsorption site
t total adsorbed phase consisting of both blocked and unblocked portions, total volume used to determine the concentration
u upstream value, unblocked portion of adsorbed phase (Appendix A), unblocked volume to determine the concentration

Superscript
* equilibrium value

Acknowledgements

We thank the National Science Foundation for support of this work through grant CTS-0442072. We also thank Remco van Soest (formerly at Dionex and currently at Eksigent) for donating several of the columns used in this study.

Appendix A. Protein adsorption equilibrium with steric hindrance effects

A steric factor that accounts for the fact that an adsorbed protein physically lies above a much larger number of charged functional groups on the column packing than is given by its characteristic binding charge has been described previously by Brooks and

Cramer [13] in their steric mass action (SMA) model. In that work, sterically blocked ion-exchange functional groups and their associated counterions were represented as undissociated ion pairs, and it was assumed that adsorbed proteins, sterically blocked sites, and unblocked sites with their associated exchangeable counterions, form a uniform, thermodynamically ideal, three-dimensional phase. More recently, it has been pointed out by Bosma and Wesselingh [31] that the SMA model assumes that the local interaction between exchangeable adsorbed counterions and a protein in the liquid phase decreases as the amount of adsorbed protein increases, even though it might be expected that these interactions should be nearly independent of the amount of protein adsorbed, in which case the SMA model predicts a slower approach to the maximum amount of adsorbed protein as the liquid-phase protein concentration is increased than would otherwise be expected.

In order to produce an alternative SMA adsorption model which approaches the maximum protein adsorption amount more rapidly than the original SMA model, especially for the case when the binding affinity is high, it will be assumed in the present study that adsorbed proteins can be visualized as being so firmly attached to the column packing that they lose their diffusional mobility and effectively become part of the column packing. Consequently, instead of assuming that an adsorbed phase exists that is uniform in composition, it is assumed that sterically blocked ion-exchange functional groups located underneath an adsorbed protein form a distinct phase separated from the remaining adsorbed phase by a hypothetical membrane that is impermeable to proteins. Adsorption equilibrium can then be determined by applying the relations in Section 3.1 first to the unblocked portion of the adsorbed phase, and then independently to the blocked portion of the adsorbed phase, with both of these adsorbed phases assumed to be in equilibrium with the same fluid phase.

According to the description just given, and using the approach of Strong [15], it follows that

$$V_t = V_u + V_b \quad \text{and} \quad n_t = n_u + n_b \tag{A1}$$

where V and n denote the volume and moles of adsorption sites per unit mass of adsorbent, respectively, and subscripts t, u, and b denote the total, the unblocked, and the blocked phase, respectively. A species concentration can be based on the total amount of a substance adsorbed per unit volume of the total adsorbed phase, or of the blocked or unblocked portions, so that

$$q_{P_i,u} = \frac{n_{P_i}}{V_u}; \quad q_{P_i,t} = \frac{n_{P_i}}{V_t} \tag{A2}$$

where the second subscript on the adsorbed-phase concentration denotes the volume used to determine the concentration. The total moles of blocked adsorption sites per unit mass of adsorbent, n_b, is given by definition as

$$n_b = \sum_{i=1}^{N_P} \sigma_i n_{P_i} \tag{A3}$$

If both sides of Eq. (A3) are divided by V_u, the result can be written as

$$q_{R_b^+,u} = \sum_{i=1}^{N_P} \sigma_i q_{P_i,u} \tag{A4}$$

The following relations are true by definition:

$$q_{R_t^+,t} = \frac{n_t}{V_t}, \quad q_{R_u^+,u} = \frac{n_u}{V_u}, \quad q_{R_b^+,b} = \frac{n_b}{V_b}, \quad q_{R_b^+,u} = \frac{n_b}{V_u}, \tag{A5}$$

$$q_{R_t^+,t} = q_{R_u^+,u} = q_{R_b^+,b} \equiv q_{R^+} \tag{A6}$$

where the subscripts R_b^+, R_u^+, and R_t^+ denote the blocked functional group sites, the unblocked functional group sites, and total amount of functional group sites, respectively. By rearranging the above relations, the following two relations result:

$$\frac{q_{R_b^+,t}}{q_{R_t^+,t}} = \frac{q_{R_b^+,u}}{q_{R_t^+,t} + q_{R_b^+,u}} \tag{A7}$$

$$\frac{q_{R_u^+,t}}{q_{R_t^+,t}} = \frac{q_{R_t^+,t}}{q_{R_t^+,t} + q_{R_b^+,u}} \tag{A8}$$

The right-hand sides of Eqs. (A7) and (A8) can be determined by recognizing that the first term in the denominator is the concentration of the charged functional groups per unit volume of total adsorbed phase, q_{R^+}, as described by Eq. (A6), while the other terms can be determined from Eq. (A4). The left side of Eq. (A7) can be interpreted as the factor which, when multiplied by a concentration per unit volume of blocked adsorbed phase, yields the concentration per unit volume of the total adsorbed phase, while the left side of Eq. (A8) can be interpreted as the analogous factor for the unblocked phase so that, with regard to the adsorbed proteins present, it follows that

$$q_{P_i,u} \cdot \frac{q_{R_t^+,t}}{q_{R_t^+,t} + q_{R_b^+,u}} = q_{P_i,t} \tag{A9}$$

For the case where a single species of protein is present, where for illustrative purposes the chloride ion is taken as the counterion, where the unblocked phase is assumed to consist of the exchangeable counterions together with the functional group sites that interact directly with adsorbed proteins, and where thermodynamic ideality for H^+ and Cl^- is assumed so that $q_{H^+}q_{Cl^-} = C_{H^+}C_{Cl^-}$, Eq. (5) leads to the following implicit equation for $q_{P,u}$:

$$C_P = \frac{q_{P,u}}{K_{P,ads}} \left(\frac{C_{Cl^-}}{q_{R^+} - z_P q_{P,u}} \right)^{z_P} \tag{A10}$$

Furthermore, for this case the relation between $q_{P,u}$ can be written explicitly in terms of $q_{P,t}$ by using Eq. (A9) to arrive at

$$q_{P,u} = \frac{q_{P,t} q_{R^+}}{q_{R^+} - \sigma q_{P,t}} \tag{A11}$$

If Eqs. (A10) and (A11) are combined to eliminate $q_{P,u}$, the result is the single component isotherm for a protein that relates $q_{P,t}$ and C_P. For the common case where $\sigma \gg z_P$ and, if $q_{P,t}$ is denoted as q_P, this result can be written as

$$C_P = \frac{q_P}{K_{P,ads}} \left(\frac{C_{Cl^-}}{q_{R^+}} \right)^{z_P} \left(\frac{q_{R^+}}{q_{R^+} - \sigma q_P} \right)^{\psi} \tag{A12}$$

where $\psi = 1$.

It is useful to recognize that the single-component SMA isotherm model described by Brooks and Cramer [13] and the single-component available area isotherm model described by Bosma and Wesselingh [31] can both also be written in the form of Eq. (A12), except that for these two cases $\psi = z_P$ and $\psi = 2.7$, respectively, as compared to the development given above where $\psi = 1$. Furthermore, since the only difference between all three of these isotherm models is the value of ψ, it follows that for a given set of values for $K_{P,ads}$, z_P, σ, and q_{R^+}, all three isotherm models have identical slopes at low protein concentrations and identical maximum adsorption capacities at high protein concentrations, but differ in the rate that the maximum amount adsorbed is approached as the fluid-phase concentration is increased, with smaller values of ψ corresponding to faster approaches to the maximum amount adsorbed.

In the present study, the approach described above leading to Eq. (A12) with $\psi = 1$ was employed to calculate protein adsorption equilibrium since this approach can be easily extended to the cases where several different proteins and buffering species

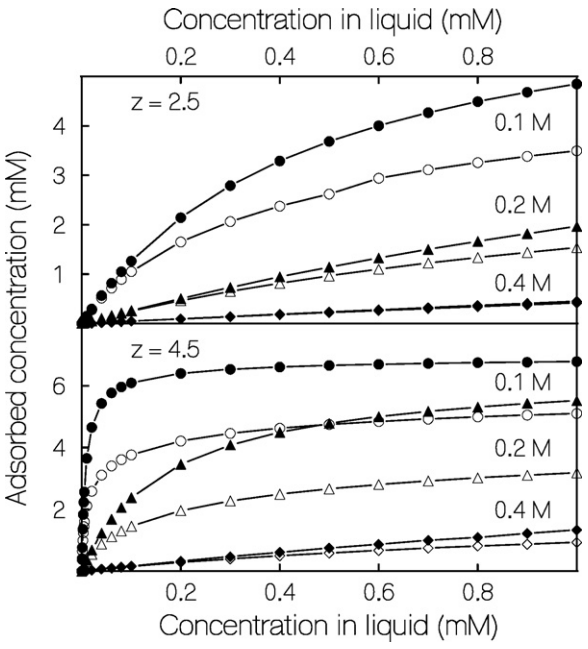

Fig. 11. Comparison between adsorption isotherms calculated from SMA model described by Brooks and Cramer (solid symbols) and from the approach described in Appendix A (open symbols). The numbers in the figure denote the ionic strengths used for the calculation. The charge states of the protein were 2.5 in the top panel and 4.5 in the bottom panel. The physical properties used for the protein and column packing were $\sigma = 100$, $K_{P,ads} = 0.1$, and $q_{R^+} = 0.75$ M.

are present which adsorb simultaneously and where the column packing functional groups are weak electrolytes whose ionization depends on the adsorbed phase pH. In addition, although the conclusions arrived at from the numerical simulations in Section 3 appear to be relatively insensitive to the choice of the parameter ψ, the maximum value of z_P in the simulations performed was large enough so that the comparatively faster approach to the maximum adsorption capacity achieved using Eq. (A12) with $\psi = 1$ was thought to better represent the true behavior. To illustrate this latter consideration, Fig. 11 compares the approach to the maximum adsorption capacity predicted by Eq. (A12) with $\psi = 1$ and with $\psi = z_P$, the latter case being the SMA isotherm of Brooks and Cramer. As shown, although the two models yield similar behavior when $z_P = 2.5$, when the value of z_P is increased to 4.5, the SMA isotherm approaches the maximum adsorption capacity of 7.5 mM significantly more slowly than Eq. (A12) with $\psi = 1$, particularly at the lowest salt concentration of 0.1 M.

Appendix B. Rules for the elution order of the buffering species in SDC

This appendix describes rules for determining the number of pH fronts formed in SDC and the buffering species that appear or disappear on each front, which are extensions of rules developed previously for ionizable [9] and nonionizable adsorbates [32]. Detailed proofs of these rules are given by Shen [33].

The first (i.e., fastest) pH front on a multistep, retained pH gradient is produced by a change in the concentration of the presaturation buffering species, and if this buffering species is not present in the elution buffer, it will then disappear on the second pH front where the first acidic buffering species in the elution buffer appears.

The following three rules apply to the remainder of the fronts and describe the appearance (i.e., an increase from zero with time) and disappearance (i.e., a decrease to zero with time) of the buffering species in the column effluent:

Rule 1: Once a buffering species disappears at a pH front, it will not reappear on any of the following (i.e., upstream) pH fronts.
Rule 2: For an anion-exchange column, the sequence of pH fronts after the first front is generated from the one-by-one appearance of the acidic buffering species present in the eluent in descending order of their pK_{A_i} values. Analogously, for a cation-exchange column, the basic buffering species present appear in the effluent in ascending order of their pK_{B_i} values. Adsorbing ions that do not participate acid-base equilibrium, such as the sodium ion for the case of a cation exchanger, appear in a front that exits the column at a later time than the fronts just described.
Rule 3: Except for the second pH front, two different buffering species cannot appear or disappear simultaneously at the same pH front.

Consequently, when there are n adsorbed buffering species present, i.e., when there are n acidic buffering species and an anion-exchange column packing is employed, there will be n pH fronts that separate $n - 1$ intermediate pH plateaus in the pH profile.

References

[1] L.A.A. Sluyterman, O. Elgersma, J. Chromatogr. 150 (1978) 17.
[2] L.A.A. Sluyterman, J. Wijdenes, J. Chromatogr. 150 (1978) 31.
[3] X. Kang, D.D. Frey, Anal. Chem. 74 (2002) 1038.
[4] R.X. Li, H. Zhou, S.J. Li, Q.H. Sheng, Q.C. Xia, R. Zeng, J. Proteome Res. 4 (2005) 1256.
[5] T. Wehr, LC–GC Eur. 22 (2004) 998.
[6] B. Herbert, P.G. Righetti, Electrophoresis 21 (2000) 3639.
[7] M. Fountoulakis, H. Langen, C. Gray, B. Takács, J. Chromatogr. A 806 (1998) 279.
[8] R.C. Bates, X. Kang, D.D. Frey, J. Chromatogr. A 890 (2000) 25.
[9] D.D. Frey, C.R. Narahari, C.D. Butler, AIChE J. 48 (2002) 561.
[10] X. Kang, D.D. Frey, J. Chromatogr. A 991 (2003) 117.
[11] C.R. Narahari, J.C. Strong, D.D. Frey, J. Chromatogr. A 825 (1998) 115.
[12] D.D. Frey, A. Barnes, J. Strong, AIChE J. 41 (1995) 1171.
[13] C.A. Brooks, S.M. Cramer, AIChE J. 38 (1992) 1969.
[14] H. Shen, D.D. Frey, J. Chromatogr. A 1034 (2004) 55.
[15] J.C. Strong, Ph.D. Thesis, University of Maryland Baltimore County, Baltimore, MD, 1997.
[16] Z.Y. Wang, M. Shimonaga, Y. Muraoka, M. Kobayashi, T. Nozawa, Eur. J. Biochem. 268 (2001) 3375.
[17] F.G. Helfferich, G. Klein, Multicomponent Chromatography – Theory of Interference, Marcel Dekker, New York, 1970.
[18] H. Shen, X. Li, C.J. Bieberich, D.D. Frey, Methods Mol. Biol. 424 (2008) 187.
[19] K. Brorson, H. Shen, S. Lute, J. Soto Pérez, D.D. Frey, J. Chromatogr. A 1207 (2008) 110.
[20] J.A. Wilkins, R. Xiang, C. Horváth, Anal. Chem. 74 (2002) 3933.
[21] R. Xiang, C. Horváth, J.A. Wilkins, Anal. Chem. 75 (2003) 1819.
[22] A. Kundu, K.A. Barnthouse, S.M. Cramer, Biotech. Bioeng. 56 (1997) 119.
[23] P.G. Righett, G. Tudor, J. Chromatogr. 220 (1981) 115.
[24] P.G. Righetti, T. Caravaggio, J. Chromatogr. 127 (1976) 1.
[25] Y.B. Yang, K. Harrison, J. Chromatogr. A 743 (1996) 171.
[26] K. Zhu, J. Zhao, D.M. Lubman, F.R. Miller, T.J. Barder, Anal. Chem. 77 (2005) 2745.
[27] A. Butt, M.D. Davison, G.J. Smith, J.A. Young, S.J. Gaskell, S.G. Oliver, R.J. Beynon, Proteomics 1 (2001) 42.
[28] S. Ghose, T.M. McNerney, B. Hubbard, Biotechnol. Prog. 18 (2002) 530.
[29] J. Soto Pérez, D.D. Frey, Biotechnol. Prog. 21 (2005) 902.
[30] D.B. Wall, M.T. Kachman, S. Gong, R. Hinderer, S. Parus, D.E. Misek, S.M. Hanash, D.M. Lubman, Anal. Chem. 72 (2000) 1099.
[31] J.C. Bosma, J.A. Wesselingh, AIChE J. 50 (2004) 848.
[32] T. Vermuelen, M.D. LeVan, N.K. Hiester, G. Klein, Perry's Chemical Engineers Handbook, McGraw-Hill, New York, 1984 (Chapter 16).
[33] H. Shen, Ph.D. Thesis, University of Maryland Baltimore County, Baltimore, MD, 2006.